Infrared Studies of Lattice Vibrations in Iron Pyrite*

J. L. VERBLE† AND R. F. WALLIS

Naval Research Laboratory, Washington, D. C. 20390

(Received 26 December 1968)

Infrared-active lattice vibrations have been studied in the cubic semiconductor iron pyrite (FeS_2) by measuring the room-temperature reflectivity at near-normal incidence. A group-theoretical analysis of lattice vibrations at the Γ point in the pyrite structure predicts five infrared-active modes belonging to the irreducible representation Γ_4^-. Four of these modes are observed experimentally. An analysis of the data using classical dispersion theory is made to determine the high-frequency dielectric constant and the frequencies, strengths, and linewidths of the observed modes. In addition, a Kramers-Kronig analysis of the data is made to obtain the dielectric response. The frequencies of four transverse and four longitudinal optical modes are also determined. The implications of the infrared data concerning the interatomic bonding in FeS_2 are discussed.

I. INTRODUCTION

INFRARED-ACTIVE lattice vibrations have been studied both experimentally and theoretically in the cubic semiconductor iron pyrite (FeS_2) in an attempt to understand the lattice dynamics and the nature of the atomic bonding in this multimode crystal. The pyrite structure, with 12 atoms per primitive unit cell, allows for 3 acoustical an 33 optical modes of vibration. By contrast, the more familiar cubic semiconductors such as Ge and Si or the III-V and II-VI compounds have structures with only two atoms per unit cell. Pyrite has also been reported[1] to have the interesting property that the elastic constant C_{12} is negative. As a first step in attempting to understand the interatomic forces in pyrite, we have undertaken a study of the infrared-active lattice vibrations.

Because of the large number of optical modes in pyrite, it is informative to determine in advance the number of modes which are expected to show infrared or Raman activity. At the same time, it is desirable to identify these vibrations according to their symmetry species or irreducible representations. Information of this type may be obtained from a group-theoretical analysis of lattice vibrations at zero wave vector ($q = 0$). In Sec. II we give the results of such an analysis as applied to the pyrite structure.

In the experimental section of this paper the room-temperature infrared reflectivity obtained from a natural specimen of FeS_2 is reported. The observed reflection spectrum is analyzed in two ways. First, the infrared-active modes are represented by damped classical oscillators. By fitting the classical oscillator theory to the observed reflectivity, the high-frequency dielectric constant and the frequencies, strengths, and linewidths of the four observed modes are determined. These results are then used to find the frequencies of the long-wavelength transverse optical (TO) and longitudinal optical (LO) modes. Secondly, a Kramers-Kronig (KK) analysis of the reflectivity data is made to obtain the dielectric response. These two methods of analysis are compared by computing in each case the refractive index, the extinction coefficient, and the real and imaginary parts of the complex dielectric function.

Finally, we discuss these results and consider how one might hope to learn more of the nature of the modes from a simple interatomic-force model.

II. STRUCTURE AND GROUP THEORY OF PYRITE

Pyrite crystallizes in a cubic structure with 12 atoms per primitive unit cell as shown in Fig. 1. The Bravais lattice is simple cubic with fundamental translation vectors

$$\mathbf{a}_1 = a_0\mathbf{i}, \quad \mathbf{a}_2 = a_0\mathbf{j}, \quad \mathbf{a}_3 = a_0\mathbf{k}, \qquad (1)$$

where a_0 is the cube edge of the unit cell and has the value[2] 5.40667 Å for FeS_2. The structure may be viewed as consisting of 12 interpenetrating simple cubic sub-
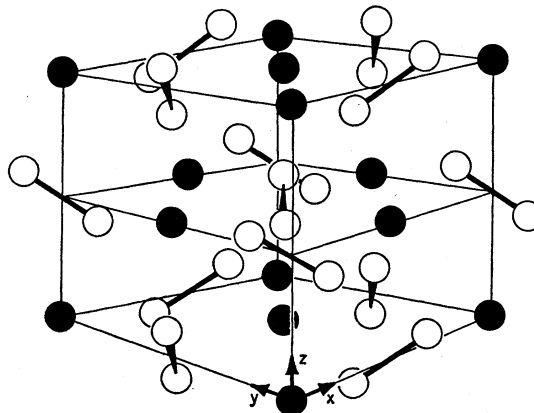
FIG. 1. Crystal structure and primitive unit cell of pyrite. The black spheres represent iron atoms, while the white spheres represent sulfur atoms.

[1] S. Bhagavantam, Proc. Indian Acad. Sci. 41A, 72(1955); S. Bhagavantam and J. Bhimasenacher, *ibid.* 20A, 298 (1944); W. Voigt, *Lehrbuch der Kristallphysik* (B. G. Teubner, Leipzig, 1938).

[2] R. W. G. Wyckoff, *Crystal Structures* (Wiley-Interscience, Inc., New York, 1963), Vol. 1, pp. 346 and 347.

TABLE I. Positions of atoms in the pyrite unit cell. The parameter u has the value 0.386 for FeS_2.

κ	Fe Coordinates	κ	S Coordinates
		5	(u, u, u)
		6	$(-u, -u, -u)$
1	$(0,0,0)$	7	$(u-\frac{1}{2}, -u+\frac{1}{2}, -u)$
2	$(0,\frac{1}{2},\frac{1}{2})$	8	$(-u+\frac{1}{2}, u-\frac{1}{2}, u)$
3	$(\frac{1}{2},0,\frac{1}{2})$	9	$(-u, u-\frac{1}{2}, -u+\frac{1}{2})$
4	$(\frac{1}{2},\frac{1}{2},0)$	10	$(u, -u+\frac{1}{2}, u-\frac{1}{2})$
		11	$(-u+\frac{1}{2}, -u, u-\frac{1}{2})$
		12	$(u-\frac{1}{2}, u, -u+\frac{1}{2})$

lattices. Four of these have iron atoms located at the lattice sites, and the other eight have sulfur atoms at the lattice sites. The sulfur atoms are positioned such that the line joining adjacent sulfur pairs is aligned along one of the four equivalent $\langle 111 \rangle$ directions.

It is of interest to note that the iron atoms in the pyrite structure sit at the sites of a fcc lattice. Likewise, if the midpoints between sulfur pairs are considered as lattice points, these also form an fcc lattice. Thus, the structure may be considered as an NaCl-like grouping of iron atoms and S_2 pairs. It should be emphasized, however, that pyrite does not have the same symmetry as NaCl, and thus one should avoid making symmetry arguments from that basis.

If the origin $(0,0,0)$ of the (x,y,z) coordinate system is chosen as shown in Fig. 1, atoms within the unit cell have the positions[3] listed in Table I. Here distances are given in units of the lattice parameter a_0. The parameter u for FeS_2 has the value 0.386.[2]

Before discussing the group analysis of pyrite, we wish to draw attention to several recent articles dealing with the application of group theory to the study of lattice vibrations. Noteworthy among these are the works of Chen,[4] of Maradudin and Vosko,[5] and of Warren.[6]

TABLE II. Factor group operations A_i of T_h^6.

i	$[R_i \mid t_i]$	i	$[R_i' \mid t_i]$
1	$[x\,y\,z \mid 0]$	1	$[\bar{x}\,\bar{y}\,\bar{z} \mid 0]$
2	$[x\,\bar{y}\,\bar{z} \mid \frac{1}{2}\frac{1}{2}0]$	2	$[\bar{x}\,y\,z \mid \frac{1}{2}\frac{1}{2}0]$
3	$[\bar{x}\,y\,\bar{z} \mid 0\frac{1}{2}\frac{1}{2}]$	3	$[x\,\bar{y}\,z \mid 0\frac{1}{2}\frac{1}{2}]$
4	$[\bar{x}\,\bar{y}\,z \mid \frac{1}{2}0\frac{1}{2}]$	4	$[x\,y\,\bar{z} \mid \frac{1}{2}0\frac{1}{2}]$
5	$[z\,x\,y \mid 0]$	5	$[\bar{z}\,\bar{x}\,\bar{y} \mid 0]$
6	$[\bar{z}\,\bar{x}\,y \mid \frac{1}{2}0\frac{1}{2}]$	6	$[z\,x\,\bar{y} \mid \frac{1}{2}0\frac{1}{2}]$
7	$[z\,\bar{x}\,\bar{y} \mid \frac{1}{2}\frac{1}{2}0]$	7	$[\bar{z}\,x\,y \mid \frac{1}{2}\frac{1}{2}0]$
8	$[\bar{z}\,x\,\bar{y} \mid 0\frac{1}{2}\frac{1}{2}]$	8	$[z\,\bar{x}\,y \mid 0\frac{1}{2}\frac{1}{2}]$
9	$[y\,z\,x \mid 0]$	9	$[\bar{y}\,\bar{z}\,\bar{x} \mid 0]$
10	$[\bar{y}\,z\,\bar{x} \mid 0\frac{1}{2}\frac{1}{2}]$	10	$[y\,\bar{z}\,x \mid 0\frac{1}{2}\frac{1}{2}]$
11	$[\bar{y}\,\bar{z}\,x \mid \frac{1}{2}0\frac{1}{2}]$	11	$[y\,z\,\bar{x} \mid \frac{1}{2}0\frac{1}{2}]$
12	$[y\,\bar{z}\,\bar{x} \mid \frac{1}{2}\frac{1}{2}0]$	12	$[\bar{y}\,z\,x \mid \frac{1}{2}\frac{1}{2}0]$

[3] *International Table for X-Ray Crystallography* (The Kynoch Press, Birmingham, England, 1952), Vol. I.
[4] S. H. Chen, Phys. Rev. **163**, 532 (1967).

From symmetry considerations alone it is possible to determine the number of infrared- and Raman-active modes of vibration and, further, to enumerate the symmetry species or irreducible representations to which these modes belong. In treating long-wavelength infrared-active vibrations we may choose $q=0$, which corresponds to vibrations at the Γ point or center of the simple cubic Brillouin zone.

Pyrite belongs[7] to the nonsymmorphic space group T_h^6 $(Pa3)$. The factor group operations A_i associated with a nonsymmorphic space group involve both a rotational part R_i and a nonprimitive translational part t_i. In Table II, we list these operations for the factor group of T_h^6.

When the T_h^6 factor group operations are applied to the coordinates of the atoms listed in Table I, one finds that the atom κ is taken into the atom κ' as given in Table III. Using Table III, one can construct a set of representation matrices[5] of order 36×36 for the symmetry point Γ. A decomposition into irreducible representations gives

$$\Gamma = \Gamma_1^+ + \Gamma_2^+ + \Gamma_3^+ + 3\Gamma_4^+ \\ + 2\Gamma_1^- + 2\Gamma_2^- + 2\Gamma_3^- + 6\Gamma_4^-. \quad (2)$$

It is well known[8] that infrared-active modes require representations with odd parity, transforming as x, y, z. The three-dimensional Γ_4^- representations meet these requirements. We thus conclude that the infrared-active modes must have this symmetry. As yet we have not considered the pure translational acoustic modes. It is easy to see, however, that these also must possess the Γ_4^- symmetry, in that they must have odd parity under inversion and transform as x, y, z. The triple degeneracy of the acoustic modes at $q=0$ implies that only one Γ_4^- representation is needed to label these modes. We are thus left with five infrared-active modes of Γ_4^- symmetry.

The Raman-active modes may be determined very simply from considering the direct product $\Gamma_4^- \times \Gamma_4^-$. This forms a reducible representation of even parity transforming as x^2, y^2, z^2, xy, etc., as required for the Raman modes. When this direct product is decomposed into irreducible representations, we find

$$\Gamma_4^- \times \Gamma_4^- = \Gamma_1^+ + \Gamma_2^+ + \Gamma_3^+ + 2\Gamma_4^+. \quad (3)$$

Since each of the Γ^+ representations is contained in this decomposition, we conclude from Eq. (2) that six modes are Raman-active, namely, one Γ_1^+, one Γ_2^+, one Γ_3^+, and three Γ_4^+.

It is impossible using infrared radiation to investigate experimentally lattice vibrations for q precisely equal to zero. Because of retardation one can only probe near

[5] A. A. Maradudin and S. H. Vosko, Rev. Mod. Phys. **40**, 1 (1968).
[6] J. L. Warren, Rev. Mod. Phys. **40**, 38 (1968).
[7] J. C. Slater, *Quantum Theory of Molecules and Solids* (McGraw-Hill Book Co., New York, 1965), Vol. 2, pp. 408–417.
[8] G. Herzberg, *Molecular Spectra and Molecular Structure* (D. Van Nostrand, Inc., New York, 1945), Vol. II.

TABLE III. Values of κ' obtained when a symmetry operation A_i is applied to atom κ.

κ	A_1	A_2	A_3	A_4	A_5	A_6	A_7	A_8	A_9	A_{10}	A_{11}	A_{12}	A_1'	A_2'	A_3'	A_4'	A_5'	A_6'	A_7'	A_8'	A_9'	A_{10}'	A_{11}'	A_{12}'
1→	1	4	2	3	1	3	4	2	1	2	3	4	1	4	2	3	1	3	4	2	1	2	3	4
2→	2	3	1	4	3	1	2	4	4	3	2	1	2	3	1	4	3	1	2	4	4	3	2	1
3→	3	2	4	1	4	2	1	3	2	1	4	3	3	2	4	1	4	2	1	3	2	1	4	3
4→	4	1	3	2	2	4	3	1	3	4	1	2	4	1	3	2	2	4	3	1	3	4	1	2
5→	5	7	9	11	5	11	7	9	5	9	11	7	6	8	10	12	6	12	8	10	6	10	12	8
6→	6	8	10	12	6	12	8	10	6	10	12	8	5	7	9	11	5	11	7	9	5	9	11	7
7→	7	5	11	9	9	7	11	5	11	7	5	9	8	6	12	10	10	8	12	6	12	8	6	10
8→	8	6	12	10	10	8	12	6	12	8	6	10	7	5	11	9	9	7	11	5	11	7	5	9
9→	9	11	5	7	11	5	9	7	7	11	9	5	10	12	6	8	12	6	10	8	8	12	10	6
10→	10	12	6	8	12	6	10	8	8	12	10	6	9	11	5	7	11	5	9	7	7	11	9	5
11→	11	9	7	5	7	9	5	11	9	5	7	11	12	10	8	6	8	10	6	12	10	6	8	12
12→	12	10	8	6	8	10	6	12	10	6	8	12	11	9	7	5	7	9	5	11	9	5	7	11

zero wave vector ($\mathbf{q} \approx 0$). In this case, it is well known that the LO modes occur at higher frequencies than their corresponding TO modes. The splittings may be attributed to a macroscopic polarization field $\mathbf{E} = -4\pi\mathbf{P}$, which is present in the case of the LO modes, but which is absent for the TO modes.

With these considerations in mind, let us again turn to the decomposition for pyrite. The Γ_4^- and Γ_4^+ representations are three-dimensional, while the remaining representations are one-dimensional. This implies a triple degeneracy for the Γ_4^- and Γ_4^+ modes and no degeneracy for the other modes. From the discussion above, however, we know that the LO and TO modes cannot be degenerate for $\mathbf{q} \approx 0$. We thus conclude that experimentally one should observe five doubly degenerate infrared-active TO vibrations. Associated with these will be five nondegenerate LO modes. For the Raman-active modes, there should be three doubly degenerate TO modes and three nondegenerate LO modes, all with Γ_4^+ symmetry; we are unable to characterize the remaining nondegenerate Γ_1^+, Γ_2^+, and Γ_3^+ modes as either TO or LO.

A final bit of symmetry information may be obtained from the fact that pyrite possesses two different centers of inversion symmetry. One inversion center is located at the sites of the iron atoms, and the second is located at the midpoint between sulfur atoms in neighboring pairs. In a mode with an even representation the displacements of particles which are related through an inversion center are in opposite directions.[9] Furthermore, particles at sites of inversion symmetry have no displacements in modes with even representations. From this we conclude that in the Γ^+ modes the iron atoms remain at rest, and the sulfur atoms in neighboring pairs move in opposite directions with equal amplitudes. Obviously, any interatomic-force model used to represent the vibrations of pyrite must reflect these symmetry requirements.

III. EXPERIMENTAL DETAILS

Measurement of the reflectivity at near-normal incidence was made at room temperature in the spectral

[9] J. Murphy, H. H. Caspers, and R. A. Buchanan, J. Chem. Phys. 40, 743 (1964).

range 190–660 cm⁻¹ using a Perkin-Elmer model 301 spectrophotometer. A natural specimen of FeS₂ with one surface highly polished was compared against an aluminized mirror, using a sample-in–sample-out procedure. Since pyrite possesses cubic symmetry, no polarization or orientation studies were necessary.

The reflectivity data are shown plotted in Fig. 2 as open circles. The solid curve drawn on the figure represents a theoretical fit to the data, which we discuss in Sec. IV. Four infrared-active modes are clearly visible in the data. The two lower-frequency modes are well separated in energy, whereas the higher-frequency modes show considerable overlap. The fifth mode which is predicted by the group theory has not been observed experimentally, even though the range of investigation was extended from 100 to 800 cm⁻¹. It seems likely then that either this mode is too weak to be observed or it is hidden by the details of the other stronger modes.

In a further attempt to observe the fifth mode, we have also studied pyrite in transmission. In this case, a thin slice of material mounted on a silicon substrate was lapped and optically polished until a sample thickness of approximately $20\,\mu$ was achieved. The sample was compared in transmission to a silicon disk identical
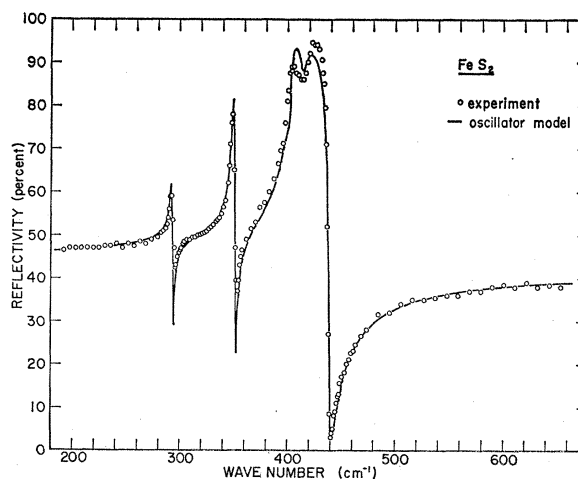
FIG. 2. Reflectivity of FeS₂ as a function of wave number. The points are experimental values, and the curve is theoretically calculated from the classical oscillator model.
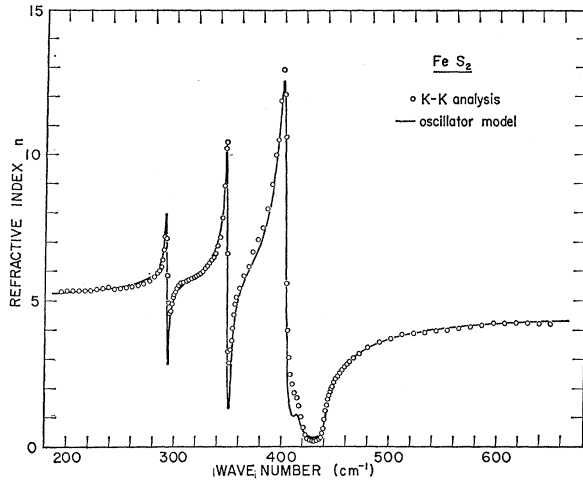
FIG. 3. Refractive index as a function of wave number. The points are obtained from a KK analysis of the reflectivity data, and the curve is theoretically calculated from the classical oscillator model.

to the one used for the substrate. The transmission study failed to reveal the fifth mode in the range 100–700 cm^{-1}. Thus, our conclusion remains that this mode is either very weak or else hidden by the other stronger modes.

IV. RESULTS AND ANALYSIS

A knowldege of the frequency dependence of the complex dielectric function $\epsilon(\omega)=\epsilon_1+i\epsilon_2$ is of central importance in understanding the optical properties of a solid. Two commonly used methods of analysis exist whereby information regarding the dielectric response of a solid may be extracted from a measured quantity such as the reflectivity. The first method involves the
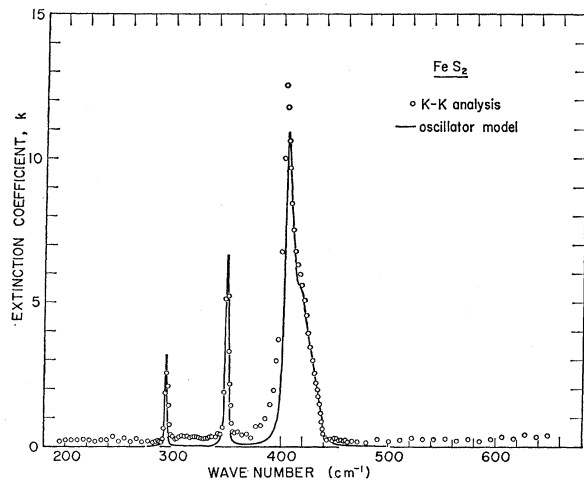
FIG. 4. Extinction coefficient as a function of wave number. The points are obtained from a KK analysis of the reflectivity data, and the curve is theoretically calculated from the classical oscillator model.

use of classical oscillator theory to represent the infrared-active modes of vibration. Barker,[10] and more recently Chang et al.,[11] have extended the macroscopic theory of Born and Huang[12] to apply to crystals with several optical modes.

Denoting the vibrational amplitude of the jth optical mode by $\mathbf{W}_j$, the equation of motion of the jth damped oscillator is written as

$$\frac{\partial^2 \mathbf{W}_j}{\partial t^2}+\gamma_j\frac{\partial \mathbf{W}_j}{\partial t}+\omega_j^2\mathbf{W}_j=\rho_j^{1/2}\omega_j\mathbf{E}. \qquad (4)$$

In addition, one can write the polarization of the crystal as

$$\mathbf{P}=\sum_j \rho_j^{1/2}\omega_j\mathbf{W}_j+\frac{\epsilon_\infty-1}{4\pi}\mathbf{E}. \qquad (5)$$

The ω_j, γ_j, and ρ_j represent, respectively, the oscillator dispersion frequency, the damping constant, and the oscillator strength of the jth mode; ϵ_∞ is the high-frequency dielectric constant; and $\mathbf{E}$ is the macroscopic electric field of the crystal. If plane-wave solutions are assumed for the quantities $\mathbf{P}$, $\mathbf{E}$, and $\mathbf{W}$, and these are then substituted into Eqs. (4) and (5), one can express the real and imaginary parts of the complex dielectric function as

$$\epsilon_1=\epsilon_\infty+\sum_j \frac{4\pi\rho_j\omega_j^2(\omega_j^2-\omega^2)}{(\omega_j^2-\omega^2)^2+(\gamma_j\omega_j\omega)^2} \qquad (6)$$

and

$$\epsilon_2=\sum_j 4\pi\rho_j\omega_j^2\frac{\gamma_j\omega_j\omega}{(\omega_j^2-\omega^2)^2+(\gamma_j\omega_j\omega)^2}. \qquad (7)$$

The reflectivity R at normal angle of incidence is related to the refractive index n and extinction coefficient k by the expression

$$R=[(n-1)^2+k^2]/[(n+1)^2+k^2], \qquad (8)$$

where $n^2-k^2=\epsilon_1$ and $2nk=\epsilon_2$. In principle, a fit to the experimental reflectivity can be obtained for a proper choice of the model parameters ω_j, ρ_j γ_j, and ϵ_∞. Adjustment of the parameters is usually made either by trial and error or by least-squares fitting of Eq. (8) to the reflectivity data.

The second method of analysis makes use of the KK transformations to determine ϵ_1 and ϵ_2 directly from the data, without reference to any model. Such an analysis can easily be carried out using a digital computer to numerically calculate the KK integral. The review article by Stern[13] contains a good discussion of the KK procedure, together with helpful hints for the construction of a workable computer program.

[10] A. S. Barker, Jr., Phys. Rev. 136, A1290 (1964).
[11] I. F. Chang, S. S. Mitra, J. N. Plendl, and L. C. Mansur, Phys. Status Solidi 28, 663 (1968).
[12] M. Born and K. Huang, Dynamical Theory of Crystal Lattices (Oxford University Press, London, 1954).
[13] F. Stern, in Solid State Physics, edited by F. Seitz and D. Turnbull (Academic Press Inc., New York, 1963), Vol. 15.

In the present work the measured reflectivity was analyzed using both the classical oscillator theory and the KK transformations. The method of analysis consisted of the following: First, attempts were made to obtain the oscillator model parameters by trial-and-error fitting of Eq. (8) to the measured reflectivity. After a reasonable fit was obtained, refinement of the parameters was made using a computer program designed to least-squares fit Eq. (8) to the data. This improved the agreement between theory and experiment in the region around the two lower-frequency modes, but little improvement was obtained for the two higher-frequency modes. Because of poor convergence, the least-squares method of fitting was somewhat unreliable. It therefore seemed desirable at this point to perform a KK analysis of the data. In Figs. 3–6 the quantities n, k, ϵ_1, and ϵ_2 computed from the KK analysis are shown represented by open circles.

Since it is the reflectivity that one observes experimentally, it could perhaps be argued that this is the quantity one should attempt to fit theoretically. On the other hand, from Eqs. (6) and (7) we observe that it is the dielectric function which is most directly related to the parameters of the oscillator theory. For this reason, we attempted to improve our oscillator fit by least-squares fitting to the real dielectric function ϵ_1 obtained from the KK analysis. The result of this is shown in Fig. 5, and the agreement is excellent. The values of the model parameters obtained from this fit are listed in Table IV. The quantities R, n, k, and ϵ_2 were then computed using these values of the parameters. The results of these calculations are shown as solid curves in Figs. 2–4 and 6.
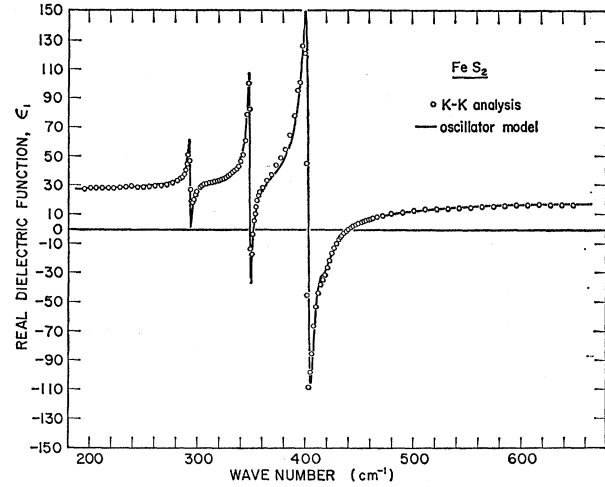
FIG. 5. Real part of the complex dielectric function versus wave number. The points are obtained from a KK analysis of the reflectivity data, and the curve is theoretically calculated from the classical oscillator model.

By splitting the phonon amplitudes W into solenoidal (transverse) and irrotational (longitudinal) parts, Chang et al.[11] show that the oscillator equations of motion (4) can be rewritten as two separate sets of equations, one for transverse modes and one for longitudinal modes. Solutions of these two sets of equations are expressed in terms of complex frequencies. The complex transverse frequencies are given by

$$S_{tj} = \pm (\omega_j^2 - \tfrac{1}{4}\gamma_j^2)^{1/2} - i\tfrac{1}{2}\gamma_j, \quad j=1, 2, \cdots, n \quad (9)$$

and the complex longitudinal frequencies are determined as solutions to the secular equation

$$\begin{vmatrix} -S_l^2 - i\gamma_1 S_l + \omega_1^2(1+4\pi\rho_1/\epsilon_\infty) & 4\pi(\rho_1\rho_2)^{1/2}\omega_1\omega_2/\epsilon_\infty & \cdots & 4\pi(\rho_1\rho_n)^{1/2}\omega_1\omega_n/\epsilon_\infty \\ & -S_l^2 - i\gamma_j S_l + \omega_j^2(1+4\pi\rho_j/\epsilon_\infty) & \cdots & 4\pi(\rho_j\rho_n)^{1/2}\omega_j\omega_n/\epsilon_\infty \\ & & \cdots & -S_l^2 - i\gamma_n S_l + \omega_n^2(1+4\pi\rho_n/\epsilon_\infty) \end{vmatrix} = 0. \quad (10)$$

Thus, if the oscillator parameters are determined, say, by fitting to the measured reflectivity, Eqs. (9) and (10) can be solved to give the TO and LO complex frequencies.

In order to determine the real parts of the TO and LO phonon frequencies, we have solved Eqs. (9) and (10) using the values of the oscillator parameters given in Table IV. These results are listed under column A in Table V.

Chang et al.[11] go on to point out that the commonly used method, wherein the LO frequencies are identified as those frequencies at which the real part of the dielectric function is equal to zero, is without theoretical justification when the oscillator model includes damping. Instead, an alternative method is developed in which the maxima and minima of the modulus of the complex dielectric function $|\epsilon| = \epsilon_1^2 + \epsilon_2^2$ are shown to yield approximately the real parts of the TO and LO

mode frequencies. The obvious advantage in using this method is that, having calculated $|\epsilon|$ from a KK or oscillator analysis, the TO and LO frequencies may be determined directly.

As a check on the frequencies obtained from Eqs. (9) and (10), the $|\epsilon|$ function has been computed using ϵ_1 and ϵ_2 determined from the KK analysis of the reflec-

TABLE IV. Values of the classical oscillator model parameters obtained from the best fit to the measured reflectivity and the ϵ_1 function computed from the KK analysis.

j	ω_j (cm⁻¹)	ρ_j	γ_j
1	293	0.0258	0.005
2	348	0.065	0.0056
3	402	0.27	0.013
4	415	0.022	0.02
$\epsilon_\infty = 21.32$		$\epsilon_0 = \epsilon_\infty + \sum_j 4\pi\rho_j = 26.13$	
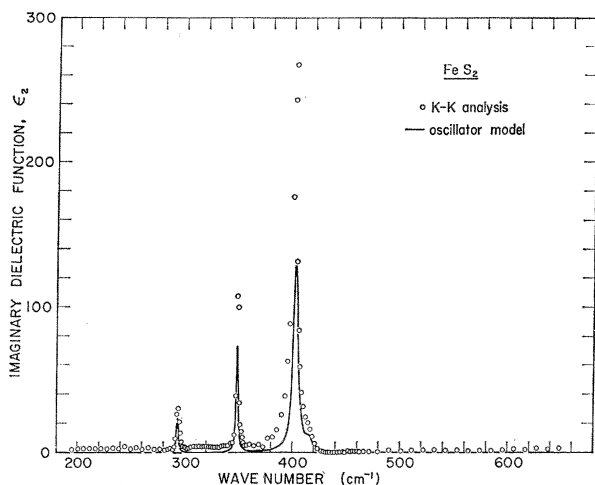
FIG. 6. Imaginary part of the complex dielectric function versus wave number. The points are obtained from a KK analysis of the reflectivity data, and the curve is theoretically calculated from the classical oscillator model.

tivity. This result is shown in Fig. 7. A smooth curve is used to connect the individual points, but has no additional theoretical significance.

One immediately observes that only three maxima and three minima are present in Fig. 7. The three maxima lead to the three TO frequencies given under column B in Table V, and the three minima lead to the LO frequencies similarly listed. These TO frequencies are in good agreement with the first, second, and third TO frequencies obtained from the oscillator fit, and, similarly, the three LO frequencies agree well with the first, second, and fourth LO frequencies listed under column A. Referring to column A, the LO mode at 414 cm^{-1} and the TO mode at 415 cm^{-1} should lead to one additional minimum and maximum, respectively,
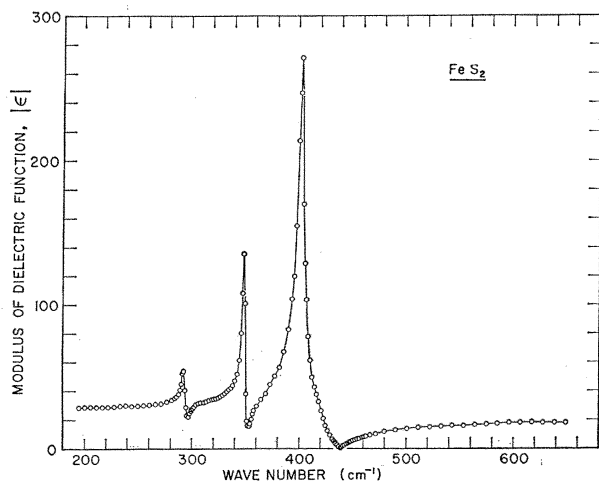
FIG. 7. Modulus of the complex dielectric function versus wave number. The points are obtained from a KK analysis of the reflectivity data. A smooth curve connects the points, but has no additional theoretical significance.

in the $|\epsilon|$ function at these frequencies. This, however, is not observed in the computed function and may be attributed to the small strength of the oscillator at 415 cm^{-1} in the presence of the strong oscillator at 402 cm^{-1}.

The results of column A of Table V demonstrate that the TO and LO modes in a multimode crystal alternate with increasing frequency. This seems to be a generally valid principle. This point has been made by Kurosawa,[14] and results from the fact that in the absence of damping the complex dielectric function possesses poles at the TO frequencies. The principle is analogous to Rayleigh's theorem as discussed by Maradudin, Montroll, and Weiss[15] for the case of a lattice perturbed by defects and impurities. There it is shown that the normal-mode frequencies of the perturbed lattice fall between those of the unperturbed lattice.

V. DISCUSSION

The classical oscillator fit to the FeS$_2$ reflectivity data is adequate in all regions except in the immediate vicinity of the two high-frequency modes. The reason for the discrepancy here is not fully understood. One possibility, which has not been taken into account by the theory, is that the fifth infrared-active mode may be present in this region. There is no experimental evidence to support this, however, either from the reflectivity or from the KK analysis of the data. Without some clear indication that the fifth oscillator is, in fact, present, its inclusion into the theory seems unwarranted.

Estep, Kovach, and Karr[16] have recently studied the infrared absorption bands of pyrite using a powdered sample suspended in a cesium iodide matrix. These authors observe four bands, and their reported absorption frequencies agree fairly well with the TO frequencies we observe in reflection. They, however, find the highest-frequency mode to be the strongest. This is in conflict with the analysis of our data which shows that mode 3 is the strongest and mode 4 is the weakest. In fitting our reflectivity data we *did* attempt to assign an oscillator strength to mode 4 larger than that for mode 3; in doing so, however, we found that we were unable to fit the broad shoulder on the low-frequency side of mode 3. In our study of the transmission, our sample was not sufficiently thin to be transmitting in the region 400–440 cm^{-1}. We are not able at this time to state whether the discrepancy between our work and that of Estep *et al.* is due to the different type of sample used or to other causes.

[14] T. Kurosawa, J. Phys. Soc. Japan 16, 1298 (1961).
[15] A. A. Maradudin, E. W. Montroll, and G. H. Weiss, in *Solid State Physics*, edited by F. Seitz and D. Turnbull (Academic Press Inc., New York, 1963), Suppl. 3.
[16] P. A. Estep, J. J. Kovach, and C. Karr, Jr., Ann. Chem. 40, 358 (1968); P. A. Estep (private communication).

TABLE V. TO and LO frequencies of the observed modes. The values in column A were obtained from Eqs. (9) and (10), and the values in column B from the maxima and minima in $|\epsilon|$.

j	A		B	
	ω_{TO} (cm^{-1})	ω_{LO}	ω_{TO} (cm^{-1})	ω_{LO}
1	293	294	292	296
2	348	352	347	353
3	402	414	402	...
4	415	439	...	440

The generalized Lyddane-Sachs-Teller relation[17] for multimode crystals in the absence of damping may be written as[18]

$$\frac{\epsilon_0}{\epsilon_\infty} = \prod_i \frac{\omega_{LOi}^2}{\omega_{TOi}^2}, \tag{11}$$

where the summation is over all the infrared-active modes. For the case of damped modes, Eq. (11) is approximately true provided the damping is small and the real parts of the complex frequencies are used. As a check on our values for the dielectric constants and the TO and LO frequencies, we have computed for the four observed modes both sides of Eq. (11) from the values given in Tables IV and V. We find $\epsilon_0/\epsilon_\infty = 1.23$ and $\prod_i \omega_{LOi}^2/\omega_{TOi}^2 = 1.22$. The agreement is thus very good and provides further evidence of the consistency of the model using four oscillators; however, it does not provide evidence about the presence or absence of the fifth unobserved mode.

The strong infrared activity of FeS₂ suggests that the interatomic bonding between iron and sulfur atoms is largely ionic in character. This is further supported by the fact that the iron and sulfur pairs form an NaCl-like structure. On the other hand, the fact that in the Raman modes the sulfur atoms in pairs vibrate against one another, while the iron atoms remain at rest, suggests that the S-S bonding is very important in determining the nature of these modes. An experimental study of the Raman-active modes would thus be of considerable interest, as this would hopefully lead to a better understanding of the S-S bonding.

As a first step toward understanding the nature of the atomic displacements in the infrared-active modes, a short-range interatomic-force model has been set up for pyrite. Using the method of de Launay,[19] we have assumed that nearest-neighboring Fe-S, S-S, and Fe-Fe

atoms interact through forces both parallel and perpendicular to the bond joining each pair of atoms. The parallel forces are specified by a central or bond-stretching force constant and the perpendicular forces by an angular or bond-bending force constant. We treat the resulting six unknown force constants as adjustable parameters in attempting to fit the model to the infrared data.

Based on this model, the dynamical matrix has been obtained for zero wave vector. For a given set of force-constant parameters the 36×36 dynamical matrix can be specified numerically. Using a computer, one can diagonalize the dynamical matrix to yield its eigenvalues and eigenvectors. By studying the atomic displacements as determined from the eigenvectors, one can identify the infrared-active modes. Attempts to fit the model to the data are made by comparing the computed and experimental frequencies as the force-constant parameters are adjusted.

As one might expect, the values of the S-S force constants are found to influence very little the frequencies of the infrared-active modes. The Raman modes, on the other hand, are expected to be very sensitive to these parameters; consequently, a knowledge of the Raman frequencies would be extremely helpful in attempting to fit the model.

Using the model described above, we have as yet been unable to obtain what we would consider a good fit to the observed infrared frequencies. This is not too surprising, however, since no account has been made for long-range electrostatic forces. A more realistic model would be one in which the ions are assumed charged and are allowed to interact via long-range Coulomb forces, as well as the previously described short-range forces. Such a model is presently under consideration in hopes of obtaining a better fit to the infrared data.

From an interatomic-force model one may, in principle, express the elastic constants of a crystal in terms of the interatomic-force constants. Our short-range force model has not given a sufficiently good fit to the infrared data to warrant this calculation for the elastic constants of pyrite. Nevertheless, provided one had an adequate model, such a calculation would be extremely useful in attempting to correlate the negative value of C_{12} to one or more of the interatomic-force constants.

ACKNOWLEDGMENTS

[17] R. H. Lyddane, R. G. Sachs, and E. Teller, Phys. Rev. 59, 673 (1941).
[18] W. Cochran, Z. Krist. 112, 465 (1959).
[19] J. de Launay, in Solid State Physics, edited by F. Seitz and D. Turnbull (Academic Press Inc., New York, 1956), Vol. 2.